High concentrations of GTP induce conformational changes in the essential bacterial GTPase EngA and enhance its binding to the ribosome

Catarina da Silveira Tomé, Anne-Emmanuelle Foucher, Jean-Michel Jault, Dominique Housset

The FEBS Journal

FEBS PRESS science publishing by scientists

High concentrations of GTP induce conformational changes in the essential bacterial GTPase EngA and enhance its binding to the ribosome

Catarina da Silveira Tomé[1], Anne-Emmanuelle Foucher[1], Jean-Michel Jault[2] and Dominique Housset[1]

1 Univ. Grenoble Alpes, CEA, CNRS, IBS, Grenoble, France
2 UMR5086 "Molecular Microbiology and Structural Biochemistry", CNRS, Univ. Lyon 1, France

Keywords
conformational change; EngA; GTPase; limited proteolysis; mass spectrometry; ribosome; small-angle X-ray scattering

Correspondence
J.-M. Jault, MMSB, 7 Passage du Vercors, F-69367, Lyon Cedex 07, France
Fax: +33 4 72 72 26 01
Tel: +33 4 72 72 26 11
E-mail: jean-michel.jault@ibcp.fr
or
D. Housset, Institut de Biologie Structurale, 71 avenue des Martyrs, CS 10090, F-38044, Grenoble Cedex 9, France
Tel: +33 4 57 42 86 18
E-mail: dominique.housset@ibs.fr

(Received 4 August 2017, revised 28 October 2017, accepted 13 November 2017)

doi:10.1111/febs.14333

EngA is a conserved bacterial GTPase involved in ribosome biogenesis. While essential in bacteria, EngA does not have any human orthologue and can thus be an interesting target for new antibacterial compounds. EngA is the only known GTPase bearing two G domains, making unique its catalytic cycle and the induced modulation of its conformation and interaction with the ribosome. We have investigated nucleotide-induced conformational changes in EngA in order to unveil their role in ribosome binding. SAXS and limited proteolysis were used to probe EngA conformational changes, and revealed a change in protein structure and a distinct rate of proteolysis induced by GTP. Structure analysis showed that the conformation adopted in solution in the presence of GTP does not match any known EngA structure, while the SAXS data measured in the presence of GDP are in perfect agreement with two crystal structures (i.e. 2HGJ and 4DCU). Combination of mass spectrometry and N-terminal sequencing for the analysis of the fragmentation pattern upon proteolytic cleavage gave insights into which regions become more or less accessible in the different nucleotide-bound states. Interactions studies confirmed a stronger binding of EngA to the bacterial ribosome in the presence of GTP and suggest that the induced change in conformation of EngA plays a key role for ribosome binding.

Introduction

Bacterial GTPases involved in the ribosome assembly form a cluster conserved throughout evolution. In comparison with well-known molecular switch GTPases, they are characterized by a moderate-to-high intrinsic GTPase activity, a low affinity for the nucleotide (K_D in the μM range) and a fast nucleotide exchange [1]. This suggests that the catalytic cycle of ribosome assembly GTPases may not be regulated by the action of GEF and GAP. Among these GTPases, six were identified as essential for cell growth: Era, RsgA, ObgE, YihA, YchF and EngA. EngA (Essential neisseria GTP-binding protein A, also known as Der, YphC or YfgK), firstly identified as a product of an essential gene for the growth of *Neisseria gonorrhoeae* growth [2], is unique among all prokaryotic and eukaryotic members of the large GTP-binding superfamily as it has two homologous and adjacent N-terminal G domains (GD1 and GD2) followed by a

Abbreviations
ELISA, enzyme-linked immunosorbent assay; FPLC, fast protein liquid chromatography; GAP, GTPase-activating protein; GEF, guanine nucleotide exchange factor; PTC, peptidyltransferase centre; SAXS, small-angle X-ray scattering.

C-terminal domain that resembles a K-homology domain (KH domain). Moreover, EngA is present and essential in several eubacterial species [3–5]. It is part of the "minimal bacterial genome" [6] and is not present in archaeal and eukaryotic organisms except in some higher plants such as *Arabidopsis thaliana* where it has a subcellular localization in chloroplasts [7]. It could thus constitute an interesting potential therapeutic target for antibacterial drugs. A link between EngA and ribosome biogenesis was first shown by Tan and collaborators [8] who demonstrated that EngA rescued a null mutation of an rRNA methyltransferase, suggesting functional interactions with the 50S subunit. Several studies in *Escherichia coli* and *Bacillus subtilis* have shown that EngA-depleted cells have decreased levels of 70S and accumulation of free ribosomal subunits 30S and 50S [9–11]. Precursors and aberrant 50S subunit were also present in such strains, indicating that EngA might play a role in the maturation and stabilization of the large ribosomal subunit [10,11].

Interaction of EngA with the 50S subunit [9,10,12,13] and with the 70S ribosome [11,13] was shown in *E. coli*, *B. subtilis* and *Mycobacterium smegmatis*, in the presence of GTP analogues. Interaction of EngA with the 30S subunit was also suggested to occur in a nucleotide-specific manner by the work of different groups [10,13], and specific interaction with the ribosomal protein S7 was shown in *Salmonella typhimurium* by both pulldown assays and ITC experiments [14]. The interaction with the 50S subunit was proposed to occur when EngA has a GD1:APO/GD2:GTP occupancy and to be further stabilized when GD1 binds GTP. When GDP is bound to GD1, however, interdomain interactions between GD1 and KH domains shift the affinity of EngA towards the 30S subunit [13]. Conversely, a study with *M. segmatis* EngA indicates that binding of EngA to the 30S occurs regardless of the presence of nucleotides [12].

Structural investigations were carried out to assess whether the nucleotide binding on either one or both EngA G domains would induce different conformations and different abilities to interact with the ribosome. All EngA structures present in the PDB are listed in Table 1. The first EngA crystal structure was obtained for *Thermotoga maritima* EngA, with two phosphate ions bound to the GD1 nucleotide-binding site and one GDP molecule bound to the GD2 nucleotide-binding site (PDB entry 1MKY, [15]). Then, structures of *B. subtilis* EngA were obtained with either GDP bound to the two G domains (PDB entries 2HJG [16] and 4DCU [17]), or with GD1 in an apo form and GMPPCP in the GD2 nucleotide-binding site (PDB entry 4DCV, [17]). While 2HJG, 4DCU and 4DCV structures are very similar, 1MKY adopts a different conformation, with a large movement of the GD1 domain relatively to the GD2-KH part of EngA, which remains unaltered. Although the GD1 nucleotide-binding site contained only two phosphate ions, this conformation was proposed to represent the GTP-bound form of EngA in several studies [15,16].

Recently, the structure of *E. coli* EngA bound to the PTC of the 50S ribosomal subunit was determined by cryo-EM (PDB entry 3J8G [18]). A mechanism was hence proposed, where EngA acts as an rRNA chaperone by binding to the PTC and facilitating its assembly. A more recent cryo-EM analysis on the large subunit from EngA-depleted *B. subtilis* [19] revealed the presence of a late-assembly 45S intermediate presenting immature conformations of the A, P and E sites, central protuberance and L7/12 stalk. Analysis of these intermediates suggested that EngA must be critical for the remodelling of RNA helices of the functional PTC core. Interestingly, the phosphate-bound form of EngA observed in 1MKY is clearly not an intermediate step between the GDP-bound form, illustrated by 2HJG and 4DCU, and the conformation of EngA adopted when bound to the 50S ribosomal subunit (3J8G). Therefore, the mechanism by which GTP could trigger a change in conformation and enhance EngA binding to the 50S subunit remains to be determined. Here, we have investigated the role of the nucleotide binding on EngA conformation in solution and its ability to enhance EngA interaction with the ribosome. Our data strongly suggest that the 2HJG

Table 1. List of EngA structures already deposited with the PDB and description of the nucleotide-binding sites content.

PDB code	Organism	Resolution (Å)	Construct	GD1 content	GD2 content	Conformation	Reference
1MKY	*Thermotoga maritima*	1.9	Full length	2 PO_4^{2-}	GDP	1MKY	[15]
2HJG	*Bacillus subtilis*	2.5	Full length	GDP	GDP	2HGJ	[16]
4DCU	*Bacillus subtilis*	2.0	Full length	GDP	GDP	2HGJ	[17]
4DCV	*Bacillus subtilis*	2.6	Full length	Empty	GMPPCP	2HGJ	[17]
3J8G	*Escherichia coli*	5.0	Full length	nd	nd	3J8G	[18]
4KYU	*Bacillus subtilis*	1.7	GD1	GDP	na	na	na

crystal structure actually represents the GDP-bound form in solution while in contrast to a previously proposed hypothesis the 1MKY structure is unlikely to represent the GTP-bound form. Combination of mass spectrometry and *N*-terminal sequencing for the analysis of the fragments produced by limited proteolytic cleavage provided insights on regions becoming more or less accessible in the different nucleotide-bound states, and suggested a timeline sequence for the GTP-induced change in conformation. Overall, our data suggest that EngA could be a sensor of GTP concentrations with observed conformational changes occurring within the range of physiological GTP concentrations, and contribute to ribosome biogenesis when this concentration is sufficiently high.

Results

GTP analogues trigger a change in conformation in solution

We have used the SAXS technique to assess the conformation of EngA in solution and to determine whether a change in conformation is induced by the presence of GTP or analogues. First, the His-EngA_{WT} in its apo form was investigated. Because a pure and monodisperse sample is of paramount importance to collect interpretable SAXS data, we looked for the presence of aggregates by carefully comparing scattering curves of apo EngA obtained either from a thawed and centrifuged sample using the automated sample changer or from a sample immediately eluted from a size exclusion chromatography column using an FPLC system directly connected to the beamline. Since the two scattering curves were nearly identical (Fig. 1A), with no indication for the presence of aggregates in the Guinier region (Fig. 1B,C), we concluded that centrifugation was sufficient to remove all possible aggregates and get a proper monodisperse sample. The Guinier analysis provided a radius of gyration of 27.1 Å and an estimated molecular mass of 37.0 kDa (Table 2). The radius of gyration is consistent with a monomeric state of EngA and close to the one calculated from the GDP-bound structure of *Bacillus subtilis* EngA, as observed in 2HJG and 4DCU PDB entries. The lower than expected estimated mass from I(0) analysis (37.0 instead of 50.8 kDa) may originate from the fact that a nucleotide could remain tightly bound to the GD2 domain. A guanine nucleotide significantly absorbs light at 280 nm (extinction coefficient $\varepsilon \approx 7720\ M^{-1}{\cdot}cm^{-1}$) and impacts the ε for His-EngA_{WT} ($33\ 350\ M^{-1}{\cdot}cm^{-1}$ without nucleotide, $41\ 070\ M^{-1}{\cdot}cm^{-1}$ with one GDP per EngA molecules). When the ε value corresponding to a EngA-1 GDP complex is used for concentration calculation, the apparent mass estimated from the Guinier analysis is 45.6 kDa, still lower to actual mass of EngA but within the ~ 10% accuracy usually observed in SAXS experiments [20]. In *T. maritima* EngA, a GDP molecule was still present in the GD2 nucleotide-binding site, even after purification steps and crystallization without nucleotides [15], indicating that the dissociation between GD2 and GDP is a very slow process. Thus, our SAXS experiment suggests that one GDP molecule might have remained tightly bound to *B. subtilis* EngA, despite the absence of nucleotide during purification process. For the sake of clarity, EngA purified without nucleotide will still be named apo EngA thereafter. The pair distance distribution calculated by the GNOM program [21] indicates a D_{max} of 93 Å and a quasi globular structure, in good agreement with available crystal structures (Fig. 2A). The CRYSOL program [21] was then used to check whether the conformation of apo EngA in solution was closer to one of the EngA conformations known so far (4DCU, 1MKY, 3J8G). The fit provides an unambiguous answer, with a very good agreement between the experimental scattering curve of apo EngA and the theoretical curve calculated from the 4DCU structure with CRYSOL ($\chi^2 = 3.16$). The fit with 1MKY and 3J8G models (χ^2 values of 32.14 and 45.32 respectively) clearly indicates that these models do not match the conformation present in solution (Table 3, Fig. 3A). Our data suggest that the apo EngA in solution, that may keep one GDP molecule bound to its GD2 domain, adopts a conformation close to the one observed in 2HJG and 4DCU crystal structures.

Next, we decided to investigate the influence of the nucleotide on the EngA conformation. Experiments were thus carried out in the presence of GDP or GTP analogues (GMPPNP and GMPPCP) at two different concentrations, 1 and 10 mM. Experimental scattering curves in the presence of GDP at either 1 or 10 mM did not show any significant difference with the one in the apo form (Fig. 4). The fit of theoretical scattering curves calculated with the 3 different EngA models with experimental curves demonstrate a very good agreement between 4DCU and EngA-GDP complex in solution (χ^2 values of 2.78 and 2.28 for 1 and 10 mM GDP respectively). Significant differences with scattering curves calculated with either 1MKY or 3J8G models were observed (Table 3). The comparison of the radius of gyration also leads to the same conclusion. For these reasons, the EngA conformation observed in 2HJG and 4DCU will be called $EngA^{apo/GDP}$ from

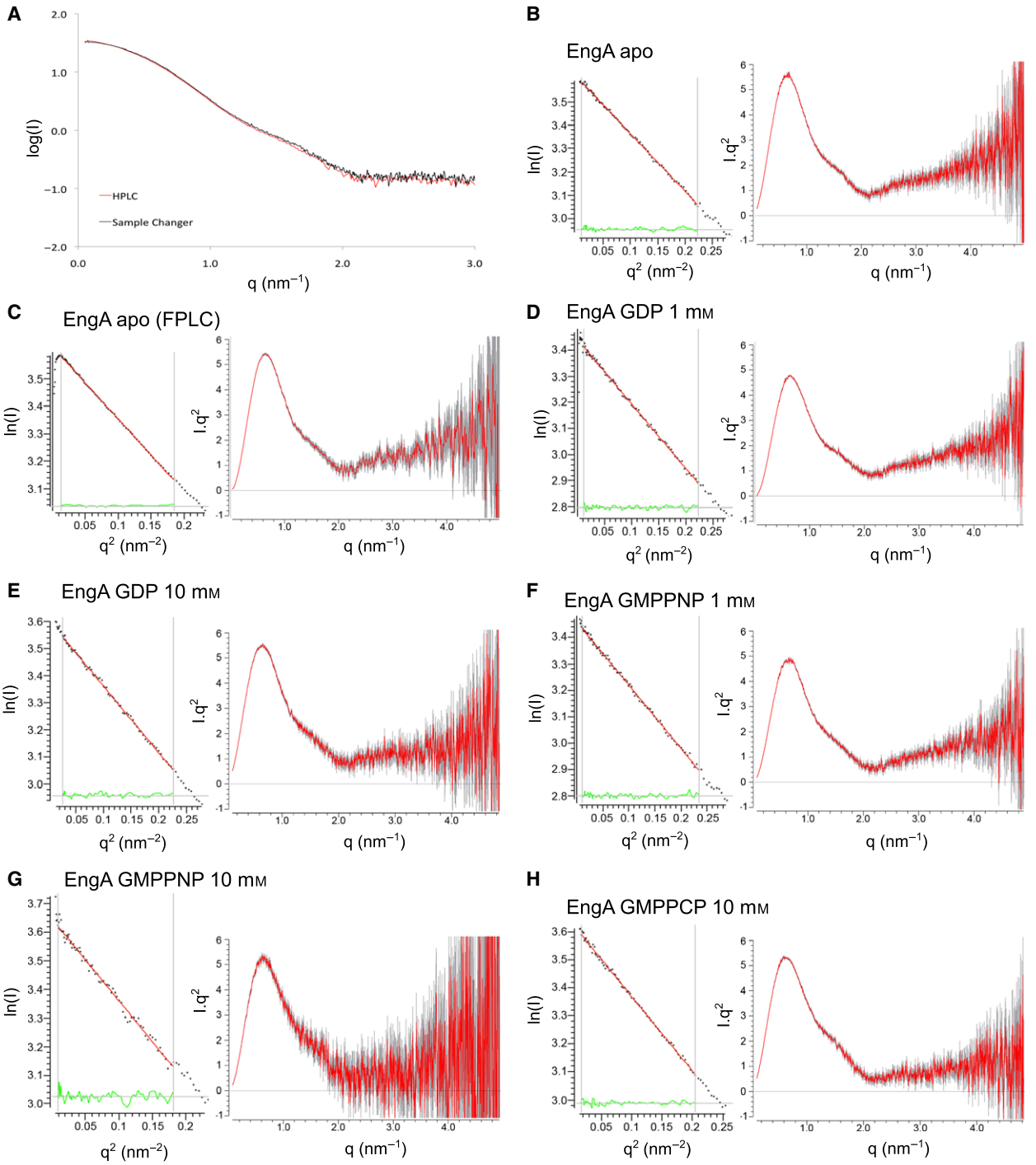

Fig. 1. (A) Comparison of apo EngA scattering curves obtained with the use of either the FPLC (red) or the sample changer (black) setup. (B–H) Guinier and Kratky plots for the different EngA samples.

now on. In the presence of GTP analogues, the experimental scattering curve depends on the nucleotide concentration. With 1 mM GMPPNP, the experimental scattering curve does not differ much from the one collected without nucleotide (apo) or in the presence of GDP (Fig. 4). The radius of gyration remains close to 27 Å and the fit with the theoretical scattering curve calculated from EngA$^{apo/GDP}$ models is significantly better than the ones based on 1MKY and 3J8G models (Table 3). In the presence of 10 mM of either

Table 2. SAXS data statistics. Structural parameters have been determined using the PRIMUS software (ATSAS suite version 2.7.2-5). The OD at 280 nm was used to estimate the protein concentration using an extinction coefficient of 33 350 $M^{-1} \cdot cm^{-1}$ (calculated with ProtParam, using the amino acid sequence of the his-tagged EngA construct).

Data collection parameters							
Beam line	ESRF BM29						
Wavelength (Å)	0.9919						
q range (nm^{-1})	0.036–5.0						
Exposure time (s)	1						
Temperature (K)	293						
EngA sample	Apo (FPLC)	Apo	1 mM GDP	10 mM GDP	1 mM GMPPNP	10 mM GMPPNP	10 mM GMPPCP
Concentration range ($mg \cdot mL^{-1}$)	1.3[a]–5.3[a]	1.2–4.8	1.0–4.2	0.93–3.0	1.0–4.8	0.31[b]–0.72[b]	0.93[b]–4.0[b]
Date of data collection	02-12-2014	02-12-2014	02-12-2014	05-10-2015	27-04-2015	14-02-2015	05-10-2015
Structural parameters							
I(0)/c [from P(r)]	36.98[a]	36.99	31.07	37.21	31.73	38.20	38.03
R_g (Å) [from P(r)]	27.9	27.1	26.9	27.5	26.8	29.0	28.5
q. R_g range for Guinier	0.32–1.21	0.28–1.29	0.28–1.28	0.44–1.29	0.27–1.30	0.27–1.25	0.37–1.28
I(0)/c [from Guinier]	37.23	37.04	31.16	37.01	31.78	38.38	37.92
R_g (Å) [from Guinier]	28.1	27.2	27.2	27.2	26.9	29.3	28.3
D_{max} (Å)	93	93	88	92	84	104	103
Porod volume estimate (nm^3)	81.5	80.4	79.4	79.9	79.1	84.8	85.4
Mass (kDa)[estimated from Porod volume]	50.9	50.3	49.6	49.9	49.4	53	53.4

[a] Since the OD could not be reliably measured with the FPLC setup on the beamline, the estimated concentration range was calculated in order to obtain the same I(0)/c as for the Apo sample.

[b] Since the OD could not be measured in the presence of 10 mM nucleotide in the buffer, the concentrations were estimated by optimizing the fit of the scattering curve with the one of the apo form.

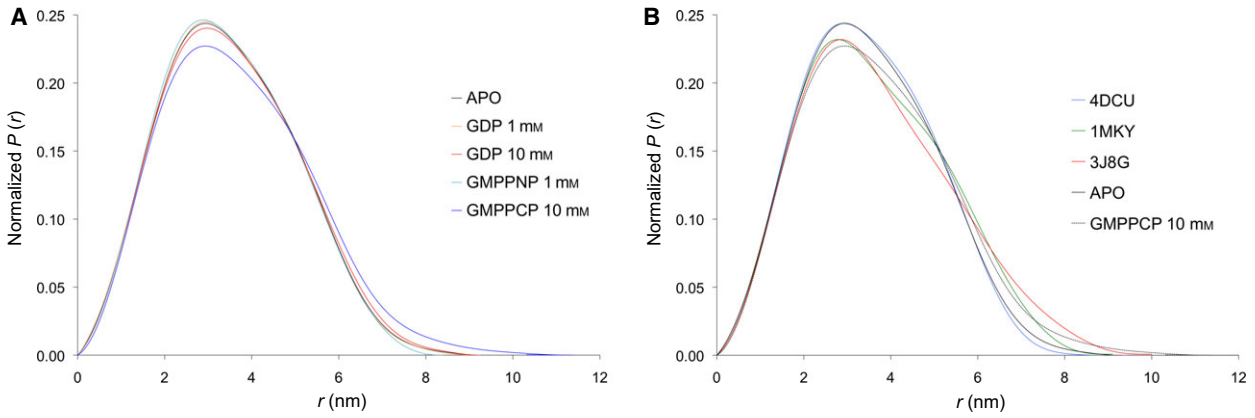

Fig. 2. (A) Interatomic distance distribution functions *P*(r) of *B.s.* EngA in the absence or in the presence of different nucleotides and at different concentrations. (B) Superposition of experimental (EngA in the apo form or in the presence of 10 mM GMPPCP) and theoretical (calculated from 1MKY, 4DCU and 3J8G PDB structures) interatomic distribution functions.

Table 3. Fitting analysis of experimental SAXS data with three models computed from PDB structures 4DCU, 1MKY and 3J8G: χ^2 represents the chi-square values and R_{gE} and R_{gT} the experimental and theoretical radius of gyration (nm) obtained for the fits. The three last columns indicate the χ^2 for the fit between models for statistical validation.

	4DCU model			1MKY model			3J8G model			4DCU/1MKY	4DCU/3J8G	1MKY/3J8G
His-EngA_{WT} form	χ^2	R_{gE}	R_{gT}	χ^2	R_{gE}	R_{gT}	χ^2	R_{gE}	R_{gT}	χ^2	χ^2	χ^2
APO	3.16	2.71	2.68	32.14	2.71	2.80	45.32	2.71	2.88	38.33	56.41	9.60
1 mM GDP	2.78	2.69	2.67	29.65	2.69	2.79	43.18	2.69	2.86	33.28	50.21	8.37
10 mM GDP	2.22	2.74	2.69	8.30	2.74	2.81	12.12	2.74	2.88	12.05	18.02	2.99
1 mM GMPPNP	2.65	2.69	2.67	24.31	2.69	2.79	32.30	2.69	2.87	26.51	37.05	6.03
10 mM GMPPNP	3.32	2.84	2.69	2.01	2.88	2.85	4.02	2.88	2.92	4.28	4.93	1.58
10 mM GMPPCP	5.13	2.79	2.69	4.41	2.79	2.85	7.77	2.78	2.93	14.73	17.28	4.76

GMPPNP or GMPPCP, the experimental scattering curve is significantly different, with a larger D_{max} and a larger radius of gyration (between 28.5 and 29 Å in comparison to 27 Å for $EngA^{apo/GDP}$, Table 2). For both GTP analogues, we could not identify a known structure that provides a perfect fit with the experimental scattering curve. The fits observed were never as good as the one observed for apo EngA or EngA-GDP and the $EngA^{apo/GDP}$ models (Fig. 3B). As shown in Table 3, the χ^2 values are smaller for 1MKY and larger for 3J8G, but none of them is as high as the calculated χ^2 values when either 4DCU and 1MKY or 4DCU and 3J8G are compared (Table 3). Therefore, the data obtained in the presence of 10 mM GMPPNP or 10 mM GMPPCP indicated that in these conditions, the EngA conformation not only differs significantly from $EngA^{apo/GDP}$ but also from the two other known conformations (1MKY and 3J8G). Thus, our SAXS data strongly suggest that a conformational change is induced when 10 mM GTP analogue are added. The analysis of the distribution of interactomic distance pairs *P*(r) further supports this hypothesis. In the presence of 10 mM of GTP analogue, the *P*(r) function is significantly different and indicates the presence of longer interactomic vectors, in agreement with a larger radius of gyration (Fig. 2B). It also significantly differs from the *P*(r) calculated with either one of the three known EngA structures. Moreover, it could not be considered as the weighted sum of two of them. Therefore, the possibility of interpreting $EngA^{GTP}$ experimental scattering by a mixture of either $EngA^{apo/GDP}$ and 1MKY or $EngA^{apo/GDP}$ and 3J8G conformations can be excluded.

High nucleotide concentration decreases EngA dynamics

Small-angle X-ray scattering enables to obtain some information about the dynamics of protein in solution by looking at the Kratky plot. For all EngA samples, the Kratky plots indicate that EngA adopts a well-folded conformation, illustrated by a bell-shaped curve (Fig. 1B–H). However, one can observe a moderate linear increase at high *q* range, suggesting the presence

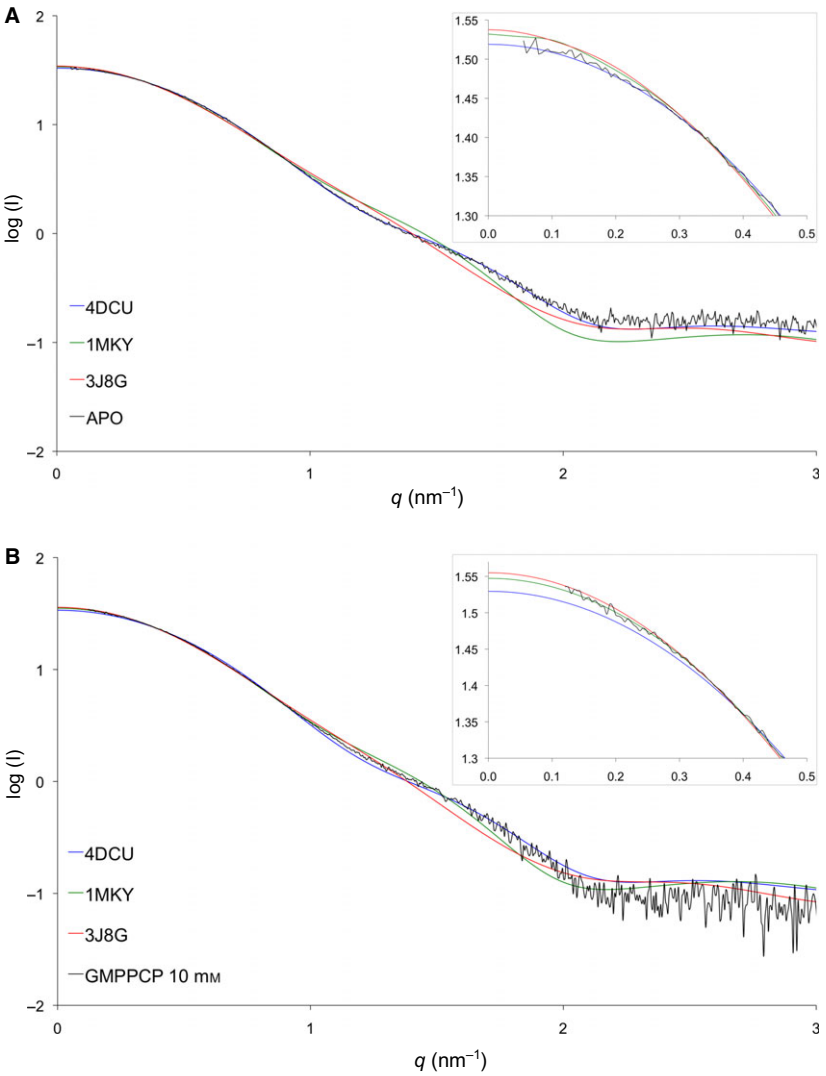

Fig. 3. Superposition of experimental (A) EngA in the apo form or (B) in the presence of 10 mM GMPPCP and theoretical (calculated from 1MKY, 4DCU and 3J8G PDB structures) interatomic distribution functions. A zoom for the low *q* values is shown in the upper-right rectangle.

of some flexible regions [22]. This is consistent with the presence of flexible switch regions in both GD1 and GD2 domains. Interestingly, the increase at high *q* range is significantly less pronounced for EngA samples that contain 10 mM of either GDP, GMPPNP or GMPPCP, suggesting the presence of high nucleotide concentration is further stabilizing EngA, regardless of its nature. Such a stabilizing effect of the nucleotide was previously observed by thermal denaturation experiments [17].

GTP analogues modulate the accessibility of trypsin cleavage sites on EngA

Limited trypsin digestion was used to investigate if a change in conformation occurs in the presence of GTP analogues. The digestion of EngA was followed over 2 h in the absence of nucleotide or in the presence of either 10 mM GDP or 10 mM GMPPCP, and resolved by SDS/PAGE (Fig. 5A). The digestion profile is basically identical for the apo EngA and EngA-GDP. The profile obtained in the presence of GMPPCP shares most of the bands seen in the apo EngA and EngA-GDP but the evolution of band intensities with time is different (see below). Mass spectrometry (MS) and N-terminal sequencing have been used to identify the fragments produced by trypsin digestion and assign the different bands observed on the gels. Mass spectrometry analysis was performed after 15 and 120 min of digestion, on the three EngA samples (apo, 10 mM GDP and 10 mM GMPPCP). Seven fragments that either end or start at a putative trypsin cleavage site could be identified (Table 4). They highlight four main cleavage sites ($^{-3}$R, ^{127}R, ^{188}K, ^{236}K/^{238}K). As seen on the SDS/PAGE, most of the fragments are found either in the absence or in the presence of nucleotides.

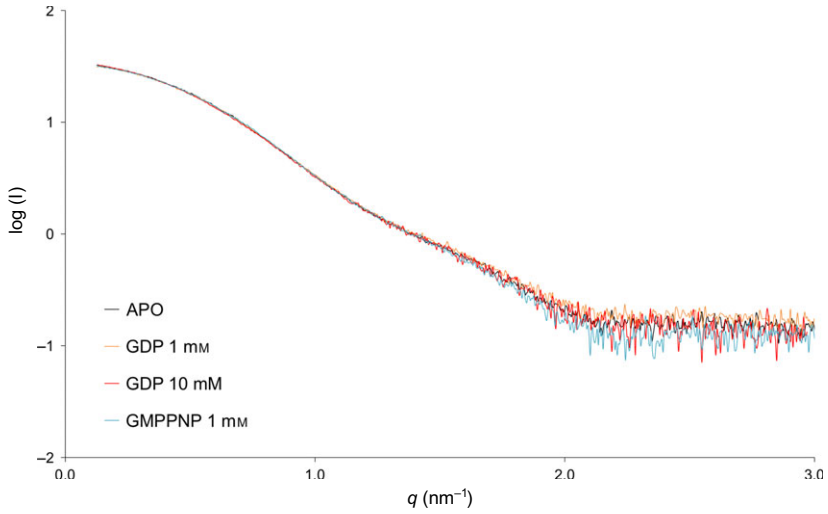

Fig. 4. Superposition of EngA scattering curves in the apo form or in the presence of 1 or 10 mM GDP or 1 mM GMPPNP.

N-terminal sequencing is globally consistent with MS analysis confirming the $^{-3}$R, ^{127}R and ^{236}K/^{238}K cleavage sites and unveiling a new one (^{345}K, Table 5). Based on the presence of five cleavage sites identified (Fig. 6A), 20 different fragments of EngA could theoretically be generated by the digestion, in addition to the full-length protein (Table 6). Twelve of these fragments could be observed on SDS/PAGE and have been assigned P1 to P12 labels. The fragments observed by mass spectrometry correspond to the most intense bands on the gels (Fig. 5A). While the cleavage sites are overall conserved, regardless of nucleotide addition, the kinetics of digestion is significantly different. In the presence of 10 mM GMPPCP, 50% of the full-length protein (P1 & P2 as they could not be properly separated on the gels) is digested in about 10 min, while in the presence of GDP or for the apo form, about 25 min are required for half digestion (Fig. 5B). No significant amount of the $^{-18}$G-^{236}K fragment (P4) is observed after 15 min in the presence of 10 mM GMPPCP, while more than 30 min are required without nucleotide or in the presence of 10 mM GDP. MS experiment confirms that the digestion of the tag fragment is significantly faster in the presence of GMPPCP, as the amount of full-length protein (P1) and *N*-terminal fragment $^{-18}$G-^{238}K (P4) remaining after 15 min digestion is not detectable. The gels also show that in addition to bands P1 and P2 that vanish more rapidly, bands P4, P5 and P6 appear earlier in the presence of GMPPCP (Fig. 5A). This is confirmed by mass spectrometry data showing that the $^{-2}$G – ^{238}K (P5) fragment is more abundant in the presence of 10 mM GMPPCP, after 15 min of digestion. Altogether, these results clearly indicate that two cleavage sites, $^{-3}$R and ^{236}K/^{238}K, are the first to be cleaved by trypsin (Fig. 6B) and are even more prone to trypsin digestion in the presence of 10 mM GMPPCP, than in the absence of nucleotide or in the presence of GDP. This suggests that the tag may be more accessible in the presence of GTP analogues than in the presence of GDP or in the apo form. The analysis of the EngA$^{apo/GDP}$ structure indicates that the access to the $^{-3}$R cleavage site by trypsin might be partially hindered by the GD1-GD2 linker and the neighbouring GD2 domain, while it seems fully accessible in the 50S ribosome-bound form (PDB entry 3J8G), in line with our digestion data (Fig. 7). Therefore, the present digestion results do support a change in quaternary structure induced by the presence of GTP analogues. Our results also suggest that the ^{236}K/^{238}K cleavage site, located in the GD2 switch II region is more accessible to trypsin. This region is well exposed to the solvent in EngA$^{apo/GDP}$. However, it is well ordered in EngA$^{apo/GDP}$, with the ^{236}K pointing towards the phosphate moiety of the nucleotide. Structural analysis of the EngA$^{apo/GDP}$ conformation indicate that the GD2 switch II region should undergo a change in conformation to allow the switch I to adopt its catalytically competent conformation. Our data suggest that in this GTP-bound conformation, the ^{236}K cleavage site is more accessible to trypsin.

In addition, another cleavage site exhibits a different behaviour, depending on the nucleotide content. The fragment $^{-2}$G–^{188}K is generated more rapidly in the presence of GMPPCP, as confirmed by both the gels (P7 band) and the mass spectrometry data at 120 min. ^{188}K is in the P-loop of the GD2 domain, and its access is partially hampered by the switch II region in EngA$^{apo/GDP}$. It thus suggests that trypsin first cleaves the GD2 switch II region and then the P-loop,

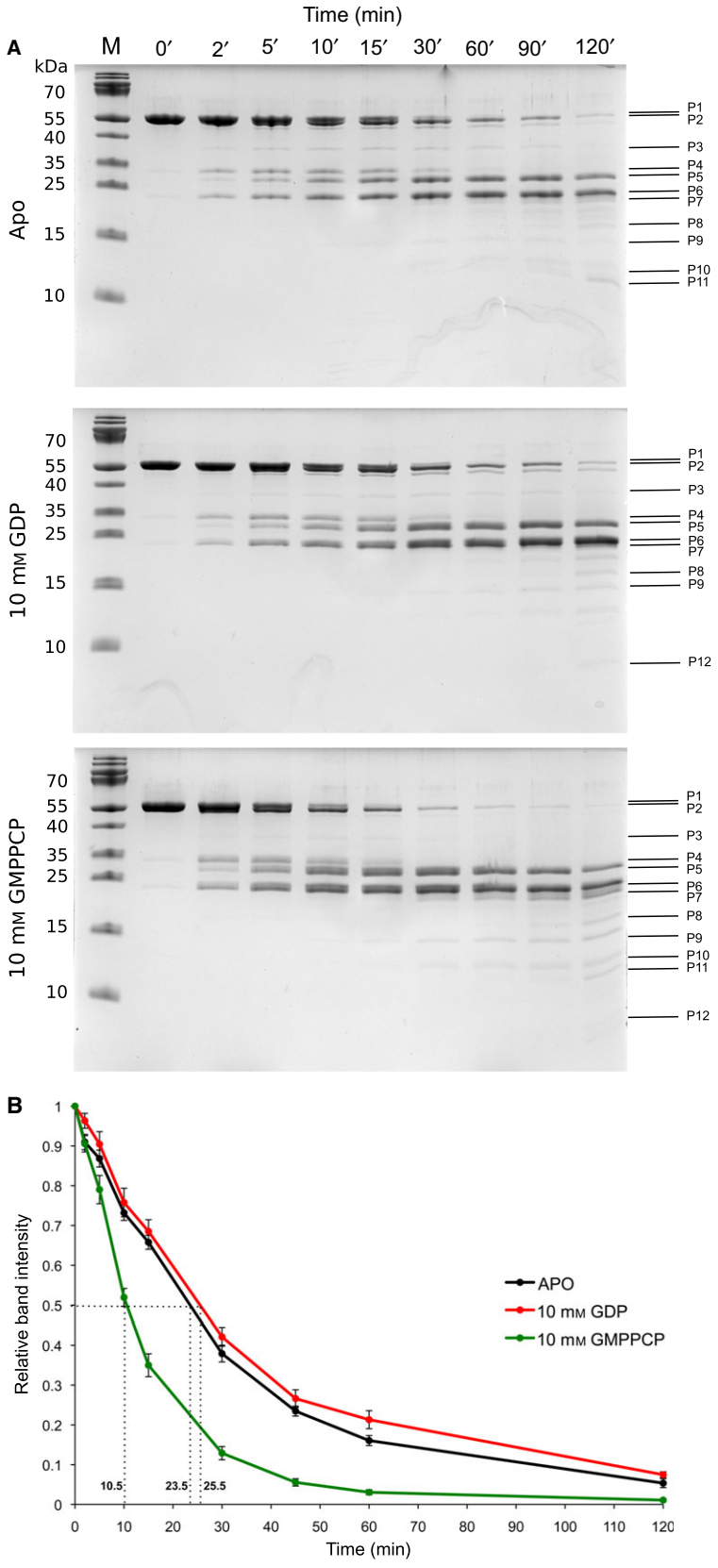

Fig. 5. (A) SDS/PAGE analysis of the tryptic digestion of His-EngA_{WT} in different nucleotide-bound states. (M) represents the molecular weight markers. (B) Analysis of the effect of nucleotides on the proteolysis rate of EngA by trypsin. The intensities of the bands on the SDS/PAGE were measured relative to time zero for the full-length EngA (P1 + P2, 100%). These values were plotted against time (min) and the t50 was determined. Each point corresponds to the mean of *n* independent sets of results and error bars represent the standard error, where *n* varies between 3 and 5.

Table 4. Peptides originated after 15 and 120 min of tryptic digestion of apo EngA and EngA-GMPPCP detected by mass spectrometry. The numbering is consistent with that of 4DCU PDB entry, with the tag spanning from −18 to 0 and the EngA protein from 1 to 436.

Time (min)	EngA	Peptides	Molecular mass (kDa)	Band identifier
15	Apo	$^{-18}$G – ^{436}K	50.805	P1
		$^{-2}$G – ^{436}K	49.051	P2
		$^{-18}$G – ^{238}K	28.214	P4
		$^{-2}$G – ^{236}K/ $^{-2}$G – ^{238}K	26.278/26.463	P5
		^{237}G – ^{435}R	22.791	P6
15	GMPPCP	$^{-2}$G – ^{436}K	49.051	P2
		$^{-2}$G – ^{236}K/ $^{-2}$G – ^{238}K	26.278/26.463	P5
		^{239}V – ^{436}K	22.606	P6
120	Apo	$^{-2}$G – ^{188}K	21.046	P7
		$^{-2}$G – ^{236}K/ $^{-2}$G – ^{238}K	26.278/26.463	P5
		^{237}G – ^{435}R/ ^{239}V – ^{436}K	22.791/22.606	P6
120	GMPPCP	$^{-2}$G – ^{127}R	14.335	P9
		$^{-2}$G – ^{188}K	21.046	P7
		$^{-2}$G – ^{236}K	26.278	P5
		^{237}G – ^{435}R/ ^{239}V – ^{436}K	22.792/22.606	P6

Table 5. Trypsin-sensitive regions detected by *N*-sequencing analysis of a digestion mix of apo-EngA_{WT} form *B. subtilis* after 15 min of digestion.

Trypsin-sensitive regions	EngA regions
$^{-3}$R/GSH^{1}MGKPV	Cleavage at C-terminal of the His_6 tag.
^{127}R/ANIYDFYS	Cleavage at C-terminal of the G4 motif of GD1.
^{236}K/GKVYETTE ^{238}K/VYETTEKY	Cleavage at the switch II region of GD2.
^{345}K/ASENHSLRV	Cleavage at the end of the last α-helix of GD2, close to the linker between GD2/KH domains.

providing a plausible explanation for the later emergence of this P7 fragment, in comparison to P4, P5 and P6. This is related to the fact that GMPPCP favour an earlier onset of this fragment, in connection with a faster digestion of the ^{236}K/^{238}K cleavage site described above.

GTP-induced conformational change is associated with enhanced ribosome binding

To examine the nucleotide-dependent binding of EngA to the ribosome, the interaction was probed in the absence and presence of GDP and GTP analogues, using an ELISA. Since our results from SAXS and trypsin digestion experiments indicated that a change in EngA conformation was observed at 10 mM GTP analogues but not at 1 mM, different nucleotide concentrations were tested in the ELISA. The GTP-bound state of EngA has been previously shown to be prone to bind to either the 50S [10] or the 70S [11] ribosome. We speculated that, if a change in conformation does relate to EngA-binding ability, an increased affinity would be observed in the presence of 10 mM GTP analogues.

The 70S ribosomes were used to coat a 96-well plate and His-EngA_{WT} was added and probed with a conjugated anti-polyhistidine antibody. The interaction curves show a nucleotide-dependent binding of EngA to the 70S ribosome (Fig. 8). Our results show that EngA is able to bind the 70S ribosome in the apo-state and that the interaction is slightly destabilized by 1 mM GDP. Such an inhibitory effect of GDP on the interaction between EngA and the ribosome had already been observed in previous studies [10,11,13]. The presence of 1 mM of either GMPPNP or GMPPCP provides a similar interaction curve to that of GDP. This suggests that 1 mM triphosphate nucleotide is not enough to induce a change in the affinity of EngA for the ribosome, consistent with SAXS data that showed that 1 mM GTP analogues were not able to trigger any conformational change. Increasing either GMPPNP or GMPPCP concentration to 10 mM greatly enhances the binding of EngA to the ribosome (Fig. 8). This strongly suggests that the conformational change observed by SAXS and limited proteolysis for EngA is associated with its ribosome binding capability. The presence of 10 mM GDP does not significantly affect the affinity for the ribosome, suggesting that the increase in binding observed with 10 mM GTP analogues is truly specific of the triphosphate nucleotide and not due to a side-effect of high nucleotide concentrations in solution.

Discussion

Conformation of the GDP- and GTP-bound form of EngA differs in solution

The GTPases are undertaking conformational changes along their catalytic cycle that influence their ability to bind with biological effectors. For monomeric GTPases, these changes are essentially confined to the two switch regions. Since EngA contains two G domains, changes in the quaternary structures may also be expected, making the switch mechanism more complex. The structure of EngA from different

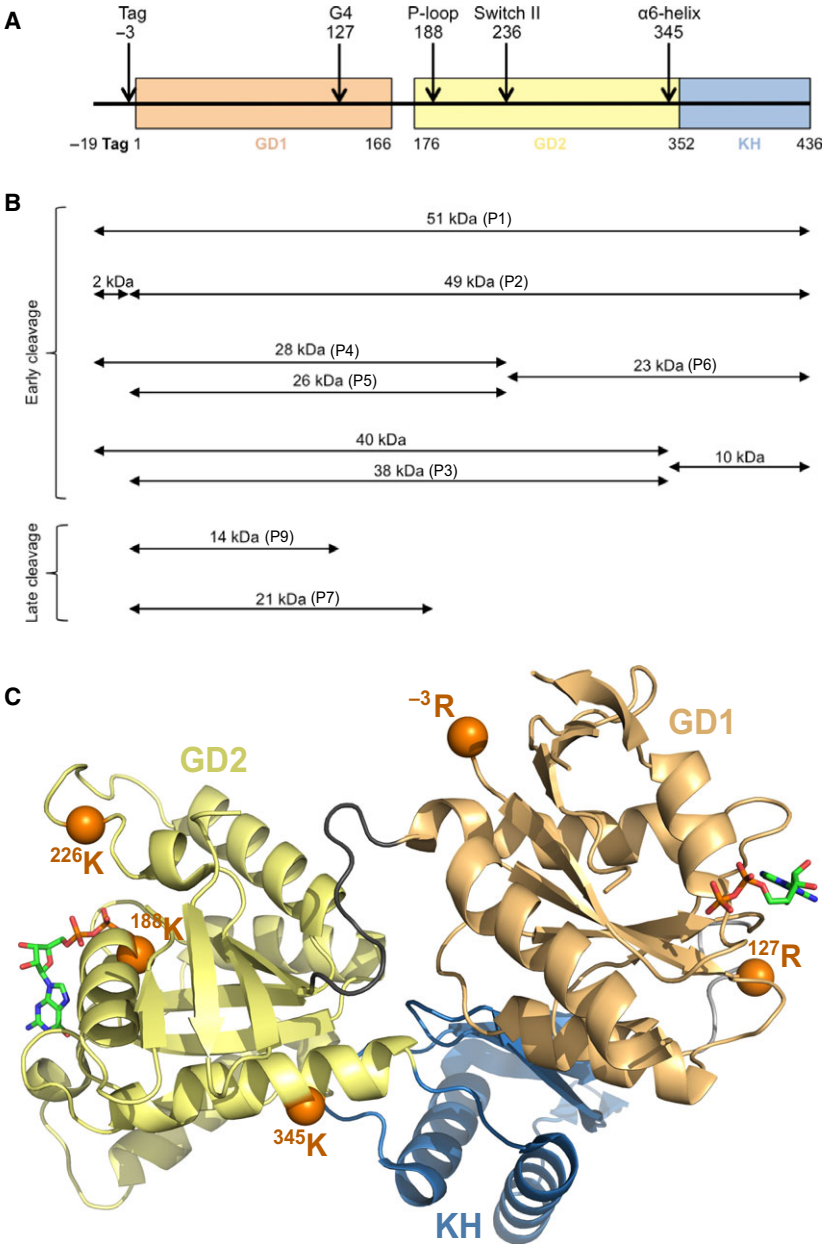

Fig. 6. (A) Schematic representation of EngA domain organization on which the five identified cleavage sites have been indicated. (B) EngA fragments observed on the SDS/PAGE gels and by MS analysis and resulting from cleavage sites $^{-3}$R, ^{236}K/^{238}K and ^{345}K (early cleavage) and ^{127}R and ^{188}K (late cleavage). (C) Position of the five cleavage sites on the EngA 3D structure. The cleavage sites are depicted by orange spheres. The 4DCU structure has been used as 3D model. GD1, GD2 and KH domains are shown in pale orange, pale yellow and blue, respectively. GD1 G4 motif (residues 122–130), not visible in 4DCU, has been modelled in light grey. The linker between GD1 and GD2 is shown in dark grey.

organisms has already been determined by either X-ray crystallography or cryo-electron microscopy in three different conformations [15–18]. However, whether these different conformations correspond to different states along the GTPase catalytic cycle or are due to difference in species, in crystallization condition or in crystal packing is a complex issue to address. In order to avoid any bias induced by the interactions within the crystal, we have investigated the structural characteristics of EngA in solution by SAXS. Our results clearly suggest that *B. subtilis* EngA either in the apo form or in the presence of GDP adopts a conformation in solution, EngA$^{apo/GDP}$, very close to that observed in the crystalline state (2HJG, 4DCU, [16,17]). It is, however, possible that what we consider to be the apo EngA already contains 1 tightly bound GDP in GD2 (see below) and thus possibly represents a GDP-bound state of EngA even without the addition of GDP. On the other hand, in a previous characterization of *B. subtilis* EngA, we showed that the addition of GDP to apo EngA triggered a large increase in the melting temperature T_m (i.e. ~ 15 °C) supporting the idea that EngA was either free from bound nucleotide or that if it already contained one tightly bound

Table 6. Theoretical mass in Daltons of *B. subtilis* EngA fragments, taking into account the cleavage sites identified by mass spectrometry experiments ($^{-3}$R, ^{127}R, ^{188}K, ^{236}K, ^{238}K) and *N*-ter sequencing (^{345}K), as calculated by ProtParam. The fragments that are observed by MS are underlined and the ones for which a band on the gel can presumably be associated with are shown in bold. When available, the MS experimentally measured mass is shown in italic.

	C-ter end of fragment						
N-ter end of fragment	$^{-3}$R	^{127}R	^{188}K	^{236}K	^{238}K	^{345}K	^{436}K
$^{-18}$G	1768.87	16085.19	22796.75	**28028.64** (P4)	**28213.86** (P4) *28214.81*	40406.93	**50801.81** (P1) *50802.59*
$^{-2}$G		**14334.33** (P9) *14334.60*	**21045.89** (P7) *21046.11*	**26277.78** (P5) *26277.94*	**26463.00** (P5) *26463.30*	**38656.07** (P3)	**49050.95** (P2) *49051.27*
^{128}A			**6729.58** (P12)	**11961.47** (P11)	**12146.69** (P11)	24339.76	34734.64
^{189}S				5249.90	5435.13	**17628.19** (P8)	28023.08
^{237}G						**12396.31** (P10)	**22791.19** (P6) *22791.49*
^{239}V						**12211.08** (P10)	**22605.96** (P6) *22606.18*
^{346}A							10412.90 *10413.38*

GDP, the saturation of the second nucleotide-binding domain by GDP (e.g. GD1) was responsible for this large increase in stability [17]. Notwithstanding this possibility, our data show that the EngA$^{apo/GDP}$ conformation corresponds to the "off" state of the enzyme, in either its apo or GDP-bound form. With the aim of triggering a change in conformation in solution, SAXS experiments were carried out in the presence of GTP analogues (GMPPNP or GMPPCP). Our results show that a concentration of 10 mM GTP analogue is required to observe a change in conformation by SAXS. The standard deviation of our SAXS data is low enough to show that unexpectedly, none of the crystal structures available perfectly match the experimental curve, since the χ^2 estimating the deviation between the experimental scattering curve and any of the three models is significantly lower than the χ^2 estimating the difference between each pair of models (Table 3). Since the experimental *P*(r) cannot be considered as a weighted average between two model *P*(r) curves (Fig. 2B), we can deduce that it also does not correspond to a mixture of known structures. Kratky plots of apo, GDP-bound and GTP-bound EngA (Fig. 1B–H) further support the presence of a stable quaternary structure as they do not show any dynamical features that could suggest the presence of a moving domain, relatively to the others. The analysis of the trypsin digestion experiments further supports our SAXS data. Among the two cleavage sites that are more rapidly cloven in the presence of 10 mM GTP analogues, $^{-3}$R and ^{236}K/^{238}K, the first one is located at the end of the N-terminal tag and is expected to be more exposed to the solvent in the GTP-bound form. Indeed, in the EngA$^{apo/GDP}$ conformation, the access to $^{-3}$R is partially hindered by the GD1–GD2 linker and the GD2 domain. This site is even less accessible to the solvent in the 1MKY EngA structure (Fig. 7), while it is fully accessible in the 3J8G structure. ^{236}K/^{238}K is in the GD2 switch II region, which should undergo a conformational change to allow GD2 to fulfil the hydrolysis of the bound GTP. The Kratky analysis of the SAXS data suggests that the EngA change in conformation upon GTP binding comes with a stabilization of EngA, precluding any increase in the flexibility that could also have supported a higher susceptibility to trypsin digestion. Altogether, these observations suggest that the GTP-bound form in solution adopts a stable conformation which has not yet been determined and is observed only when the GTP concentration reaches 10 mM.

The GTP-bound conformation of EngA in solution appears significantly different from the conformation observed when bound to the 50S ribosome (3J8G structure), although both were obtained in the presence of GTP analogues and may represent the "on" state of EngA. The EngA-50S complex structure

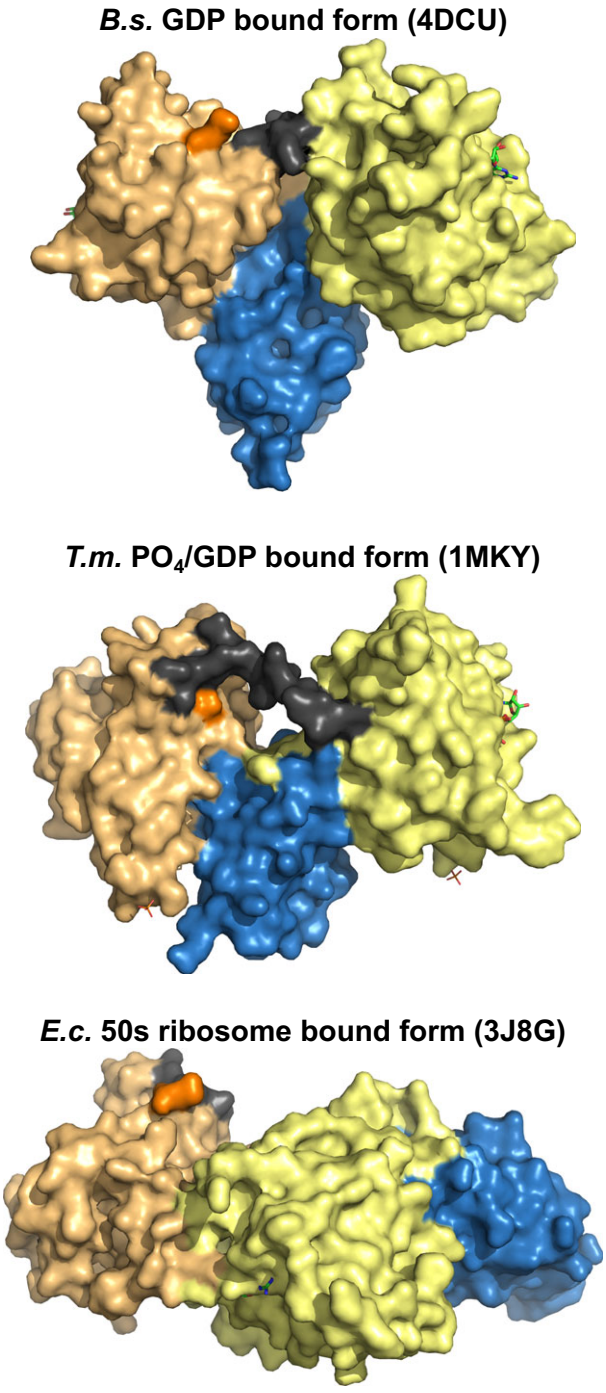

Fig. 7. Solvent accessibility of the EngA N-terminal end. The molecular surface of *Bacillus subtilis* GDP-bound form (top, PDB entry 4DCU), *Thermotoga maritima* PO_4 ions/GDP-bound form (middle, PDB entry 1MKY) and *Escherichia coli* 50S ribosome-bound form (bottom, PDB entry 3J8G) is depicted in gold (GD1 domain), yellow (GD2 domain) and blue (KH domain). The linker between GD1 and GD2 is shown in dark grey and the N-terminal residue is shown in orange.

(3J8G) clearly indicates that the $EngA^{apo/GDP}$ conformation is not compatible with a similar mode of docking to the 50S ribosomal subunit since several GD1 residues that are involved in the GD1/KH interface in the $EngA^{apo/GDP}$ conformation are forming interaction with the L1 protein and the RNA in the 3J8G structure. Both our SAXS and trypsin digestion data strongly suggest that the presence of the GTP analogue is able to induce a quaternary structural change in EngA, in which the GD1/KH interface is disrupted. The observed difference in radius of gyration leads us to suggest that the GTP-bound conformation observed in solution may represent an intermediate state between the $EngA^{apo/GDP}$ and the ribosome-bound state. This GTP-bound state may be prone to bind the 50S ribosomal subunit, provided additional conformational adjustments occur upon interaction with ribosomal components.

Our data do not support the hypothesis made in several studies [13,15,16,23] that 1MKY could correspond to the GTP-bound EngA conformation. The different conformation observed in 1MKY may come from the different crystal packing and/or from the different crystallization conditions. In fact, the crystallization solution contains 2 M sodium-potassium phosphate that certainly explains the presence of the two phosphate ions in the GD1 nucleotide-binding site. Moreover, this very high ionic concentration may have contributed to the disruption of the GD1/KH interface observed in the $EngA^{apo/GDP}$ conformation, that essentially relies on acidic (GD1) or basic (KH) amino acids [16].

The GTP concentration that induces a change in conformation also enhances the interaction with the ribosome

Our data indicate that similar levels of GTP concentration are required to either induce a conformational change on EngA or increase the binding of EngA to the ribosomes. The need of 10 mM nucleotides to induce a change in conformation may seem unexpected given the effect of nucleotides on ribosome binding observed by other groups using lower concentrations (0.1–1 mM, [10–13]). The difference may come from the fact that the apo EngA produced for the present study seems to retain GDP bound to the GD2 domain. Thus, a higher GTP concentration may be required to perform the exchange with the bound GDP molecule. Interestingly, the GTP pool has been determined in *E. coli* as being in the order of the

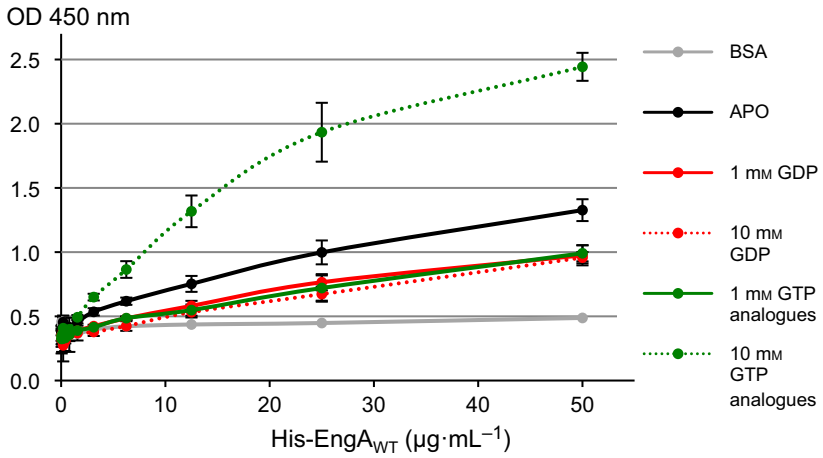

Fig. 8. Interaction between His-EngA$_{WT}$ and 70S ribosome measured by ELISA. The purified *B. subtilis* 70S ribosome was used to coat a 96-well plate. EngA was incubated with different nucleotides prior to addition to the coated wells. "GTP analogues" refers to samples tested with either GMPPNP or GMPPCP, which gave identical results and thus were analysed as one. OD_{450} values were plotted against EngA concentration (μg·mL^{-1}). Each point corresponds to the mean of *n* independent sets of results and error bars represent the standard error where *n* varies between 2 and 6 depending on the samples.

millimolar range (1.7–4.9 mM) [24,25] and can be subjected to large variations in response to different stimuli: from 0.4 mM up to GTP levels over 10 mM [26], while the GDP concentration remains more stable in the 0.1–0.7 mM range [24,25]. Our data indicate that, in the presence of bound GDP on EngA, the critical GTP concentration to induce a conformational change in EngA and an increase in its affinity for the ribosome is in the 1–10 mM range. Altogether, this suggests that EngA can be an efficient sensor of these variations in GTP intracellular concentration and modulate its interactions with the ribosome according to it. Indeed, previous observations had suggested that EngA, as well as other ribosome assembly GTPases, could be involved in sensing nucleotide concentrations to regulate ribosome synthesis according to the cell requirements [27,28]. Here, we show that EngA may switch from the "off" to the "on" state and modulate its ability to interact with the ribosome within the range of GTP concentration observed *in vivo*.

Nucleotide affinity for GD1 and GD2 nucleotide-binding sites

Our SAXS data would be consistent with the conclusion that a GDP molecule remains bound to *B. subtilis* EngA after the purification steps performed without any nucleotide. This observation suggests that one of the G domains has a high affinity for GDP. In *T. maritima*, a GDP molecule was observed bound to the GD2 domain, while the purification and the crystallization steps were performed without nucleotide [15]. For *B. subtilis*, all crystal structures obtained so far contain either GDP or GTP analogues in the GD2 domain. When present in the crystallization solution, phosphate or sulphate ions efficiently compete with GDP for the GD1 nucleotide-binding site. As a consequence, GDP is observed in the GD1 nucleotide-binding site only if the crystallization buffer does not contains any phosphate or sulphate ion. Moreover, GTP has never been seen bound to the GD1 of *B. subtilis* EngA, even with GTP analogue concentration as high as 10 mM (data not shown), suggesting a very low affinity of the GD1 for GTP when EngA is in the EngA$^{apo/GDP}$ conformation. Available structural data provide further support for a low affinity for the GD1 nucleotide-binding site, since in the context of the full-length protein, the G4 motif of the GD1 domain is always disordered [16,17], hampering its role in stabilizing the guanine base of the nucleotide through the conserved aspartic acid side chain. Therefore, all these observations strongly suggest that as for *T. maritima*, *B. subtilis* EngA possesses a low-affinity nucleotide-binding site in the GD1 domain and a high-affinity binding site in the GD2 domain.

From GTP-induced switch rearrangements to change in quaternary structure

Two phenomena can possibly monitor the sensitivity of EngA to 1–10 mM GTP concentrations: the low affinity of the GD1 domain for the nucleotide and/or the high affinity of the GD2 domain for GDP that may prevent rapid exchange between GDP and GTP. Structural data confirm that GDP/GTP exchange in the GD2 domain is obtained in the above mentioned range of GTP concentration [17]. The trypsin digestion data presented here also indicate that the GD2 switch II adopts a new conformation in the presence of GTP, in line with the fact that switch II loop conformation observed in EngA$^{apo/GDP}$ has to move for a proper

positioning of the switch I region for the catalysis. Thus, the most probable hypothesis is that the binding of GTP to GD2 will trigger a change in both the switch II GD2 conformation, enabling the GD2 switch I to adopt a conformation compatible with the hydrolysis of the GTP. Then, the change in EngA quaternary structure will occur. Whether the hydrolysis of the GD2-bound GTP is required for this change in conformation to occur and how the structural changes in the GD2 could trigger the loosening of the GD1 and KH domains interface remain unknown. Nevertheless, this change in EngA conformation may in turn induce some changes in the affinity of GD1 for the nucleotide. Cooperativity between GD1 and GD2 has already been suggested by GD2 mutations affecting significantly the enzymatic activity of the whole enzyme, while the activity of the GD1 has been shown to account for most the whole EngA activity [9,17]. Consistent with a possible cooperativity, the behaviour of the isolated GD1 domain seems different from the one in the context of the whole protein. A structure of *B. subtilis* EngA GD1, recently deposited in the PDB (4KYU) shows that the G4 motif is ordered and stabilizes the guanine base in a canonical fashion. Such an observation supports the GDP/GTP affinity for the *B. subtilis* GD1 construct, found to be in the μM range [17]. Binding of GTP to GD1 may stabilize the GD1 switch regions and thereby facilitate the binding with 50S ribosomal subunit.

Materials and methods

EngA production and purification

Wild-type *B. subtilis* EngA was cloned into a pET15b vector overexpressed as described in [11]. Purification was performed using a protocol similar to the one described in [17]. In brief, after overexpression for 4 h at 37 °C, the harvested cells were resuspended in 20 mL lysis buffer (50 mM Tris-HCl pH 8, 250 mM NaCl, 10 mM imidazole, 1 mM PMSF, 1 mM DTT, 2 $\mu g \cdot mL^{-1}$ DNAse I) and lysed using a microfluidizer (three cycles, 15 000 psi). The lysate was then centrifuged for 45 min at 30 000 ***g*** at 4 °C to remove cell debris. The supernatant was applied onto a Ni-nitrilotriacetic acid agarose column equilibrated with a washing buffer (50 mM Tris-HCl pH 8.0, 250 mM NaCl, 20 mM imidazole). The resin was washed with 10 column volumes washing buffer, and the protein was eluted using 5 column volumes of elution buffer (50 mM Tris-HCl pH 8.0, 250 mM NaCl, 300 mM imidazole, 10% glycerol). EngA was further purified by size exclusion chromatography using a HiLoad™ 26/60 Superdex™ 75 prep grade from GE Healthcare equilibrated in 50 mM Tris-HCl pH 8.0, 250 mM NaCl, 10% glycerol, used as storage buffer. Fractions containing EngA were pooled and concentrated using Vivaspin centrifugal concentrator with a cut-off of 30 kDa until a final concentration of ~ 4 $mg \cdot mL^{-1}$ estimated by measuring the OD at 280 nm, using an extinction coefficient 33 350 $M^{-1} \cdot cm^{-1}$, as calculated by ProtParam [29].

Ribosomes production and purification

Ribosomes were purified from a culture of *Bacillus subtilis* grown in LB medium at 37 °C until a final OD at 600 nm of 0.6. *B. subtilis* cells were harvested by a 20 min centrifugation at 1800 ***g*** and 4 °C. Cells were resuspended in 20 mL buffer A (20 mM Tris-HCl pH 7.5, 20 mM $MgCl_2$, 200 mM NH_4Cl, 0.1 mM EDTA, 6 mM β-mercaptoethanol, 1 mM PMSF, 1 $U \cdot mL^{-1}$ DNAse I) and disrupted using a microfluidizer (three cycles, 1000 bars). A 25-min centrifugation at 50 000 ***g*** and 4 °C was carried out to remove cell debris. The supernatant was then centrifuged 3.5 h at 240 000 ***g*** and 4 °C, generating two pellets: a clear one, on the bottom, formed by ribosomes and a brown one, on top, formed by membrane proteins. The two pellets were resuspended in buffer A, loaded on top of a 42% sucrose cushion prepared in buffer B (20 mM Tris-HCl pH 7.5, 10 mM $MgCl_2$, 500 mM NH_4Cl, 0.1 mM EDTA, 6 mM β-mercaptoethanol) and centrifuged 16 h at 130 000 ***g*** and 4 °C. Ribosomes were found in the pellet while the rest of the components remained in solution. The purified ribosomes were resuspended in buffer C (20 mM Tris-HCl pH 7.5, 10 mM $MgCl_2$, 50 mM NH_4Cl, 0.1 mM EDTA, 6 mM β-mercaptoethanol), fast frozen in liquid nitrogen and kept at −80 °C until use. Individual 30S and 50S subunits were obtained by dialysing the purified ribosomes in buffer D (20 mM Tris-HCl pH 7.5, 3 mM $MgCl_2$, 300 mM NH_4Cl, 0.15 mM EDTA, 2 mM DTT) overnight at 4 °C. The sample was then loaded onto a 5–20% sucrose gradients prepared in buffer D and centrifuged 15 h at 77 000 ***g*** and 4 °C. Fractions of 300 μL were collected in 96-well plates and the OD at 260 and 280 nm was measured in a plate reader. The fractions corresponding to each subunit were gathered and dialysed in buffer E (20 mM Tris-HCl pH 7.5, 10 mM $MgCl_2$, 50 mM KCl, 0.1 mM EDTA, 1 mM DTT) using an Amicon Ultra centrifugal concentrator (Millipore) with a cut-off of 100 kDa. Quantification of the ribosomes was accomplished by OD at 260 nm, using the following values: an OD of 1 at 260 nm corresponds to 23 pmol of 70S ribosomes, 34.5 pmol of 50S subunit and 69 pmol of 30S subunit [30].

Limited proteolysis by trypsin

Limited proteolysis of His-$EngA_{WT}$ was performed at 20 °C in 50 mM Tris-HCl pH 8.0, 250 mM NaCl and using an enzyme to substrate ratio of 1 : 600. The assay was

performed after incubation of EngA for 15 min at 37 °C in the absence of nucleotides or in the presence of 10 mM GDP/$MgCl_2$ or 10 mM GMPPCP/$MgCl_2$. Aliquots were collected at time intervals and the reaction stopped by the addition of 2 × denaturing loading dye and incubation at 95 °C for 10 min. The digestion pattern was visualized by Tricine-SDS/PAGE on 15% acrylamide gels stained with Coomassie brilliant blue G-250 solution. The gels were processed for fragment analysis using ImageJ 1.49 and Image-LabTM 4.0 softwares. Mass spectrometry (MS) analysis was employed for identification of the fragments generated by tryptic cleavage of His-$EngA_{WT}$. MS analysis was done by electrospray ionisation (ESI) coupled to a time-of-flight (TOF) mass spectrometer, using the system 6210 LC-ESI-TOF (Agilent Technologies). In addition, N-terminal amino acid sequence determination of fragments in solution was done using the Procise® Sequencing system 492 (Applied Biosystems), based on the Edman degradation reaction. N-terminal residues were identified using a 140C HPLC system (Applied Biosystems). Retention times and integration values of peaks were compared to the chromatographic profile of a standard mixture of derivatized amino acids.

ELISA

The interaction of His-$EngA_{WT}$ and 70S ribosome was assessed by a direct ELISA. The 70S ribosome was diluted in 10 mM Tris-HCl pH 7.5, 60 mM KCl, 10 mM $MgCl_2$ to a final concentration of 24 nM. The wells of a 96-well plate Maxisorb Nunc-Immuno F96 (Nunc) were coated with 50 μL 70S solution for 2 h at room temperature under agitation. The wells were then blocked with 300 μL of TBS buffer (50 mM Tris-HCl pH 7.6, 150 mM NaCl) complemented with 3% BSA and 10 mM $MgCl_2$ at 4 °C, overnight. His-$EngA_{WT}$ was diluted in TBS/Tween-20 0.05% to a range of increasing concentrations. His-$EngA_{WT}$ was preincubated 15 min at room temperature in the absence of nucleotides or in the presence of 1 or 10 mM of either GDP/$MgCl_2$, GMPPNP/$MgCl_2$, or GMPPCP/$MgCl_2$. Fifty microlitres of His-$EngA_{WT}$ were added to the wells and the plate was incubated for 2.5 h at room temperature under agitation. Binding of His-$EngA_{WT}$ was probed with a monoclonal anti-polyHistidine antibody peroxidase conjugate (Sigma-Aldrich) diluted to 1 : 2000 in TBS/Tween-20 0.05% complemented with 10 mM $MgCl_2$. Detection was done by addition of 100 μL of 3,3′,5,5′-tetramethylbenzidine (TMB) (Sigma-Aldrich) followed by a 1 h incubation at room temperature. The reaction was stopped by addition of 200 μL of H_2SO_4 0.5 M and absorbance was read at 450 nm.

Sample preparation for Small angle X-ray scattering

Frozen recombinant EngA were thawed and centrifuged for 30 min at 16 000 ***g*** and 4 °C. A PD10 gel filtration column (GE Healthcare) was used to exchange the $EngA_{WT}$ storage buffer to 50 mM Tris-HCl (pH 8.0), 250 mM NaCl. This buffer was used as a reference for SAXS experiments and for preparing sample dilutions to obtain a range of protein concentrations between 0.5 and 4 $mg{\cdot}mL^{-1}$.

Nucleotide-bound proteins were dialysed using a Vivaspin concentrator (Sartorius) with buffer containing $MgCl_2$ and GDP or GTP analogues (GMPPNP and GMPPCP) at 1 mM and 10 mM. The flow-through was used as the reference for SAXS experiments and for preparing sample dilutions. Because the presence of nucleotide interferes with visible absorption spectroscopy at 280 nm (epsilon value), OD estimate could not reliably be used and protein concentration was estimated based on successive dilution and concentration steps. Concentrations were further confirmed by I_0 values obtained from SAXS scattering curve analyses.

Data collection and processing

Small angle X-ray scattering data were collected at the BM29 beamline (ESRF, Grenoble, France) [31] using a Pilatus 1M detector. The detector-distance of 2.9 m covers a momentum transfer range of $0.025 < q < 5\ nm^{-1}$. SAXS experiments were carried out at 20 °C with sample concentrations ranging from 0.5 to 4 $mg{\cdot}mL^{-1}$ and sample volumes of 50 μL in a quartz glass capillary, using the automated sample changer. For each protein sample, data from the corresponding buffer was collected to provide a reference for the scattering background. For each measurement, ten frames were collected for which radiation damage was systematically investigated. One experiment was carried out on the apo form of the wild-type EngA using the online FPLC size exclusion purification system, in order to detect the possible presence of aggregates. As no difference was observed between scattering curves obtained with the FPLC setup and the sample changer, the latter one was used for all the experiments.

Data processing was done with the ATSAS suite of programs [21] using the installation provided by SBGRID [32]. The forward scattering I_0 and the radius of gyration Rg were calculated using the Guinier approximation using PRIMUS. The calibration of the beamline was made with pure water and in such a way that I_0/c indicates the apparent molecular weight in kDa. The distance distribution function $P(r)$ and maximum dimensions Dmax were calculated using GNOM. Fitting of the experimental data and the theoretical scattering curves computed from the PDB structures 4DCU, 1MKY and 3J8G was done using CRYSOL. Statistical validation of the fitting analysis was done by evaluation of the χ^2 values between the different models. For samples containing nucleotides, we observed that the concentration of nucleotide in the sample and the buffer did not exactly match, despite dialysis or the use of the concentration flow-through as reference buffer. Therefore,

a scattering curve for the nucleotide $I_{nucleotide}(q)$ was measured by subtracting scattering curves corresponding to the buffer containing nucleotide and buffer without nucleotide. Then, a program was written to estimate the difference in nucleotide content between the buffer and the sample. The program calculates the α and β coefficients in order to minimize the χ^2 value:

$$\chi^2 = \Sigma_q(I_{sample}(q) + \beta.I_{nucleotide}(q) - I_{buffer}(q) - \alpha.I_{model}(q))^2 / (\sigma(I_{sample}(q))^2 + \sigma(I_{buffer}(q))^2 + \sigma(I_{nucleotide}(q))^2)$$

with I_{model} being the theoretical scattering intensity of one of the available EngA crystal structures (PDB entries 4DCU, 1MKY or 3J8G), calculated by CRYSOL. The χ^2 is calculated in the q range 0.8–2.5 nm^{-1} where the fit between measured and calculated scattering curves is optimal. The corrected experimental scattering curve for the nucleotide-bound EngA is then $I_{sample}(q) + \beta.I_{nucleotide}(q) - I_{buffer}(q)$. For all the samples, the final scattering curve used for analysis is obtained by merging measurements made from at least three different concentrations, in which intensities for low q values were contributed by low concentration measurements and intensities for high q values by high concentration measurements.

Acknowledgments

We acknowledge the European Synchrotron Radiation Facility (ESRF) for provision of synchrotron radiation facilities and we thank Petra Pernot and Martha Brennich for assistance in using the SAXS beamline BM29. We acknowledge the platforms of the Grenoble Instruct centre (ISBG; UMS 3518 CNRS-CEA-UGA-EMBL) supported by the French Infrastructure for Integrated Structural Biology Initiative FRISBI (ANR-10-INSB-05-02) and by the Grenoble Alliance for Integrated Structural Cell Biology GRAL (ANR-10-LABX-49-01) within the Grenoble Partnership for Structural Biology (PSB). We would like to thank Jean-Pierre Andrieu (N-terminal sequencing) and Luca Signor (Mass spectrometry) for their assistance in data analysis. J-MJ thanks the financial support from the ANR (ANR-12-BSV3-0008-02). This work was supported by a PhD fellowship from the Commissariat à l'énergie atomique et aux énergies alternatives (CEA, IRTELIS PhD program) to CST.

Author contributions

CST, AEF, JMJ and DH designed the studies and analysed the results. CST performed all the experiments with the help of AEF for EngA/Ribosome interaction assays and DH for SAXS data collection and processing. JMJ and DH supervised the project. DH wrote the manuscript with inputs from all authors. All authors reviewed the results and approved the final version of the manuscript.

References

1 Verstraeten N, Fauvart M, Versées W & Michiels J (2011) The universally conserved prokaryotic GTPases. *Microbiol Mol Biol Rev* **75**, 507–542.
2 Mehr IJ, Long CD, Serkin CD & Seifert HS (2000) A homologue of the recombination-dependent growth gene, rdgC, is involved in gonococcal pilin antigenic variation. *Genetics* **154**, 523–532.
3 Hwang J & Inouye M (2001) An essential GTPase, der, containing double GTP-binding domains from *Escherichia coli* and *Thermotoga maritima*. *J Biol Chem* **276**, 31415–31421.
4 Morimoto T, Loh PC, Hirai T, Asai K, Kobayashi K, Moriya S & Ogasawara N (2002) Six GTP-binding proteins of the Era/Obg family are essential for cell growth in *Bacillus subtilis*. *Microbiology* **148**, 3539–3552.
5 Zalacain M, Biswas S, Ingraham KA, Ambrad J, Bryant A, Chalker AF, Iordanescu S, Fan J, Fan F, Lunsford RD *et al.* (2003) A global approach to identify novel broad-spectrum antibacterial targets among proteins of unknown function. *J Mol Microbiol Biotechnol* **6**, 109–126.
6 Mittenhuber G (2001) Comparative genomics of prokaryotic GTP-binding proteins (the Era, Obg, EngA, ThdF (TrmE), YchF and YihA families) and their relationship to eukaryotic GTP-binding proteins (the DRG, ARF, RAB, RAN, RAS and RHO families). *J Mol Microbiol Biotechnol* **3**, 21–35.
7 Suwastika IN, Denawa M, Yomogihara S, Im CH, Bang WY, Ohniwa RL, Bahk JD, Takeyasu K & Shiina T (2014) Evidence for lateral gene transfer (LGT) in the evolution of eubacteria-derived small GTPases in plant organelles. *Front Plant Sci* **5**, 678.
8 Tan J, Jakob U & Bardwell JCA (2002) Overexpression of two different GTPases rescues a null mutation in a heat-induced rRNA methyltransferase. *J Bacteriol* **184**, 2692–2698.
9 Bharat A, Jiang M, Sullivan SM, Maddock JR & Brown ED (2006) Cooperative and critical roles for both G domains in the GTPase activity and cellular function of ribosome-associated *Escherichia coli* EngA. *J Bacteriol* **188**, 7992–7996.
10 Hwang J & Inouye M (2006) The tandem GTPase, Der, is essential for the biogenesis of 50S ribosomal subunits in *Escherichia coli*. *Mol Microbiol* **61**, 1660–1672.
11 Schaefer L, Uicker WC, Wicker-Planquart C, Foucher AE, Jault JM & Britton RA (2006) Multiple GTPases participate in the assembly of the large ribosomal subunit in *Bacillus subtilis*. *J Bacteriol* **188**, 8252–8258.

12 Agarwal N, Pareek M, Thakur P & Pathak V (2012) Functional Characterization of EngAMS, a P-Loop GTPase of *Mycobacterium smegmatis*. *PLoS ONE* **7**, e34571.
13 Tomar SK, Dhimole N, Chatterjee M & Prakash B (2009) Distinct GDP/GTP bound states of the tandem G-domains of EngA regulate ribosome binding. *Nucl Acids Res* **37**, 2359–2370.
14 Lamb HK, Thompson P, Elliott C, Charles IG, Richards J, Lockyer M, Watkins N, Nichols C, Stammers DK, Bagshaw CR *et al.* (2007) Functional analysis of the GTPases EngA and YhbZ encoded by *Salmonella typhimurium*. *Protein Sci* **16**, 2391–2402.
15 Robinson VL, Hwang J, Fox E, Inouye M & Stock AM (2002) Domain arrangement of Der, a switch protein containing two GTPase domains. *Structure* **10**, 1649–1658.
16 Muench SP, Xu L, Sedelnikova SE & Rice DW (2006) The essential GTPase YphC displays a major domain rearrangement associated with nucleotide binding. *PNAS* **103**, 12359–12364.
17 Foucher A-E, Reiser J-B, Ebel C, Housset D & Jault J-M (2012) Potassium acts as a GTPase-activating element on each nucleotide-binding domain of the essential *Bacillus subtilis* EngA. *PLoS ONE* **7**, e46795.
18 Zhang X, Yan K, Zhang Y, Li N, Ma C, Li Z, Zhang Y, Feng B, Liu J, Sun Y *et al.* (2014) Structural insights into the function of a unique tandem GTPase EngA in bacterial ribosome assembly. *Nucl Acids Res* **42**, 13430–13439.
19 Ni X, Davis JH, Jain N, Razi A, Benlekbir S, McArthur AG, Rubinstein JL, Britton RA, Williamson JR & Ortega J (2016) YphC and YsxC GTPases assist the maturation of the central protuberance, GTPase associated region and functional core of the 50S ribosomal subunit. *Nucleic Acids Res* **44**, 8442–8455.
20 Mylonas E & Svergun DI (2007) Accuracy of molecular mass determination of proteins in solution by small-angle X-ray scattering. *J Appl Crystallogr* **40**, s245–s249.
21 Petoukhov MV, Franke D, Shkumatov AV, Tria G, Kikhney AG, Gajda M, Gorba C, Mertens HDT, Konarev PV & Svergun DI (2012) New developments in the ATSAS program package for small-angle scattering data analysis. *J Appl Crystallogr* **45**, 342–350.
22 Rambo RP & Tainer JA (2011) Characterizing flexible and instrinsically unstructured biological macromolecules by SAS using the Porod-Debye Law. *Biopolymers* **95**, 559–571.
23 Majumdar S, Acharya A, Tomar SK & Prakash B (2016) Disrupting domain-domain interactions is indispensable for EngA-ribosome interactions. *Biochim Biophys Acta* **1865**, 289–303.
24 Buckstein MH, He J & Rubin H (2008) Characterization of nucleotide pools as a function of physiological state in Escherichia coli. *J Bacteriol* **190**, 718–726.
25 Bennett BD, Kimball EH, Gao M, Osterhout R, Van Dien SJ & Rabinowitz JD (2009) Absolute metabolite concentrations and implied enzyme active site occupancy in *Escherichia coli*. *Nat Chem Biol* **5**, 593–599.
26 Kriel A, Bittner AN, Kim SH, Liu K, Tehranchi AK, Zou WY, Rendon S, Chen R, Tu BP & Wang JD (2012) Direct regulation of GTP homeostasis by (p) ppGpp: a critical component of viability and stress resistance. *Mol Cell* **48**, 231–241.
27 Britton RA (2009) Role of GTPases in bacterial ribosome assembly. *Annu Rev Microbiol* **63**, 155–176.
28 Karbstein K (2007) Role of GTPases in ribosome assembly. *Biopolymers* **87**, 1–11.
29 Gasteiger E, Hoogland C, Gattiker A, Duvaud S, Wilkins MR, Appel RD & Bairoch A (2005) Protein identification and analysis tools on the ExPASy server. In The Proteomics Protocols Handbook (Walker JM, ed), pp. 571–607. Humana Press, Totowa, NJ.
30 Daigle DM & Brown ED (2004) Studies of the interaction of *Escherichia coli* YjeQ with the ribosome *in vitro*. *J Bacteriol* **186**, 1381–1387.
31 Pernot P, Round A, Barrett R, De Maria Antolinos A, Gobbo A, Gordon E, Huet J, Kieffer J, Lentini M, Mattenet M *et al.* (2013) Upgraded ESRF BM29 beamline for SAXS on macromolecules in solution. *J Synchrotron Radiat* **20**, 660–664.
32 Morin A, Eisenbraun B, Key J, Sanschagrin PC, Timony MA, Ottaviano M & Sliz P (2013) Cutting Edge: collaboration gets the most out of software. *Elife* **2**, e01456.